

Converting Underwater Imaging into Imaging in Air

Tim Dolereit^{1,2} and Arjan Kuijper³

¹Fraunhofer Institute for Computer Graphics Research IGD, Joachim-Jungius-Str. 11, 18059 Rostock, Germany

²University of Rostock, Institute for Computer Science, Albert-Einstein-Str. 22, 18059 Rostock, Germany

³Fraunhofer Institute for Computer Graphics Research IGD, Fraunhoferstr. 5, 64283 Darmstadt, Germany

Keywords: Underwater Image Formation, Underwater Camera Model, Camera Calibration, Underwater Stereo Vision.

Abstract: The application of imaging devices in underwater environments has become a common practice. Protecting the camera's constituent electric parts against water leads to refractive effects emanating from the water-glass-air transition of light rays. These non-linear distortions can not be modeled by the pinhole camera model. For our new approach we focus on flat interface systems. By handling refractive effects properly, we are able to convert the problem to imaging conditions in air. We show that based on the location of virtual object points in water, virtual parameters of a camera following the pinhole camera model can be computed per image ray. This enables us to image the same object as if it was situated in air. Our novel approach works for an arbitrary camera orientation to the refractive interface. We show experimentally that our adopted physical methods can be used for the computation of 3D object points by a stereo camera system with much higher precision than with a naive in-situ calibration.

1 INTRODUCTION

The almost standard installation of visual sensors on autonomous underwater vehicles (AUV) or remotely operated vehicles (ROV) and the possibility to also equip divers with them, makes underwater imaging an efficient sampling tool. Some of the key advantages of underwater imaging are its non-destructive behavior toward marine life and its repeatable application.

Imaging underwater imposes different constraints and challenges than imaging in air. One of the main problems is the refraction of light passing bounding, transparent interfaces between media with differing refractive indexes (water-glass-air transition). In this paper we focus on flat interface systems. Such systems can be cameras watching through a viewing window, an aquarium, etc. or cameras inside a special housing immersed in water. A severe effect induced during this transition is that objects seem to be closer to the observer and hence bigger than they actually are (see figure 1). This refraction induced deviation in dimension is dependent on the distance of the imaged objects to the refractive interface and the incidence angle of light rays entering the camera through this interface. This dependency acts in a non-linear way and poses a problem to every discipline relying upon metric image information.

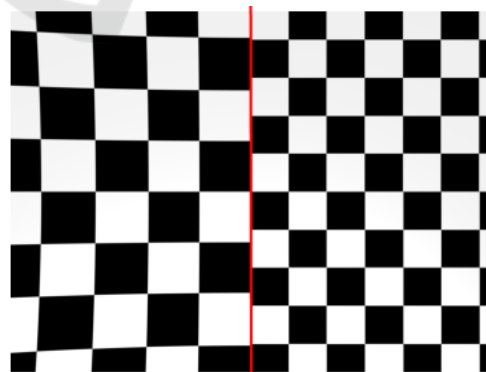


Figure 1: left - exemplary magnification and distortion underwater, right - perspective imaging in air.

If it is the task to gain metric information from the recorded images, the cameras have to be calibrated and the refractive effects have to be handled in a way to prevent the calibration of getting corrupted. The mapping of a camera from the imaged three-dimensional scene of the world to the two-dimensional image plane can be well approximated using the linear pinhole camera model of perspective projection. This is represented by a set of intrinsic camera parameters (focal length, image principal point, skew factor). As no camera, respectively no real lens is expected to fulfill this linear mapping per-

fectly, some non-linear terms are incorporated into the calibration process accounting for radial and tangential distortions. Because of the well known fact, that underwater images have multiple viewpoints (Treibitz et al., 2012), calibration of cameras imaging underwater scenes is theoretically not possible with the pinhole camera model. Nevertheless, many works have been published using a standard in air calibration technique. Despite the fact that the imaging model does not match the imaging conditions, they have to deal with an often cumbersome handling of calibration targets by divers underwater. This is accompanied by a severe loss of expensive underwater dive time, which is supposed to be used for the actual tasks that have to be performed.

In this paper we present a method to convert underwater imaging to the conditions in air. After application of this novel approach it is possible to use well known computer vision algorithms suitable for in air usage based on the pinhole camera model. Using our approach, the camera parameters can now be calibrated with a standard technique in air, followed by a step in which the corrected parameters can be derived. To achieve this, we compute virtual camera parameters following the pinhole model per image ray based on rules of physical optics. These parameters vary for image rays with differing properties. Once computed, the set of virtual parameters is reusable for every new view acquired with the calibrated camera. As a result, we get a virtual center of projection, a virtual focal length and an orientation of the virtual camera to the refractive interface for each ray respectively. This essentially converts the underwater imaging problem into imaging in air as will be explained in the later sections. Our approach works for cameras oriented arbitrarily to the refractive interface.

In section 2 a brief overview on related works is given. Section 3 describes the problems we have to deal with. A short overview of our approach is presented and our imaging setup is explained. Section 4 deals with the computations needed in our approach. In section 5 an experiment on stereo 3D reconstruction incorporating the results of section 4 is described. Our results – outperforming a naive in-situ calibration – are presented in section 6 and section 7 deals with conclusions and future works.

2 RELATED WORK

In this section a brief overview on underwater imaging using flat interface systems and handling refraction in relation to camera calibration is given. A comprehensive overview on camera models in underwater

imaging can be found in (Sedlazeck and Koch, 2012).

The first kind to handle refraction is by simply using the pinhole camera model. Refractive effects are either completely ignored (Gracias and Santos-Victor, 2000; Pessel et al., 2003; Kunz and Singh, 2010; Brandou et al., 2007; Pizarro et al., 2009; Silvatti et al., 2012) or expected to be absorbed by the non-linear distortion terms (Shortis and Harvey, 1998; Shortis et al., 2009; Meline et al., 2010; Eustice et al., 2008). Further similar approaches using in-situ calibration strategies are mentioned in (Brandou et al., 2007; Beall et al., 2010; McKinnon et al., 2011; Johnson-Roberson et al., 2010; Sedlazeck et al., 2009).

The second kind to handle refractive effects is to model them explicitly and incorporate them into the camera model and calibration process. The reasoning concerning the applicability of the pinhole model in imaging through refractive media by many authors is that it is invalid. For that reason, refraction is modeled physically correct (Agrawal et al., 2012; Chang and Chen, 2011; Chari and Sturm, 2009; Gedge et al., 2011; Ishibashi, 2011; Ke et al., 2008; Kunz and Singh, 2008; Kwon and Casebolt, 2006; Li et al., 1997; Maas, 1995; Sedlazeck and Koch, 2011; Joridt-Sedlazeck and Koch, 2012; Telem and Filin, 2010; Treibitz et al., 2012; Yamashita et al., 2006).

A different way to handle refraction is by approximation. Belonging into this category, (Ferreira et al., 2005) assume only low incidence angles of light rays on the refractive surface. The approach with the most similar aim is perhaps the work of (Lavest et al., 2003). They try to infer the underwater calibration from the in air calibration in form of an approximation of a single focal length and radial distortion. The inapplicability of the pinhole model is not considered.

In contrast to the above methods, we try to infer the underwater camera parameters following the pinhole camera model ray-based for multiple viewpoints from in air camera parameters. Furthermore, no cumbersome in-situ handling of calibration targets is needed.

3 PROBLEM STATEMENT

The main contribution of this paper is a way to relate an image of an object immersed in water with an image of the same object as if it was situated in air. This makes the application of the well known pinhole camera model of perspective projection possible. As already stated in other works like (Treibitz et al., 2012), we also assume that the pinhole camera model is not valid in underwater imaging setups. As can be

seen in figure 2, the extension of the refracted image rays (dashed lines) into air leads to several intersection points, depending on the respective incidence angles, representing multiple virtual viewpoints (red dots). Because of refraction, there is no collinearity between the object point in water, the center of projection of the camera (black dot) and the image point. On the contrary, all rays following the pinhole camera model intersect in a single point, namely the center of projection. This occurrence of multiple virtual viewpoints in underwater imaging makes it impossible to infer a single focal length adjustment that can represent the imaging situation in terms of the pinhole camera model correctly. Nevertheless, a relation between the two imaging situations can be assembled for the single image rays. It follows the rules of physical optics and is presented in the following sections.

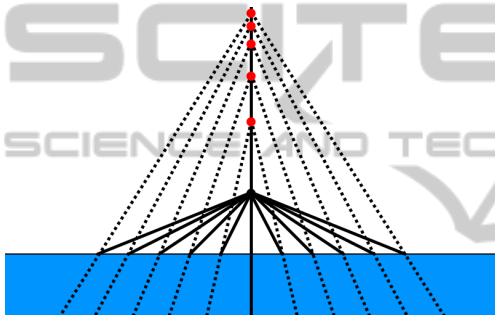


Figure 2: Multiple viewpoints in underwater imaging.

3.1 Overview

The main idea of our approach is, that the imaging camera with a constant focal length is working based on the pinhole camera model. In essence, it does not know anything about refraction. Hence (see figure 3), one can assume that the camera is imaging a virtual object point V , which is situated collinear to the camera's center of projection P and the image point I . The real object point O is not situated collinear, as a result of refraction known from Fermat's and Snell's law. We assume that the camera's intrinsics and non-linear distortion terms in air are known. For now, it is expected that lens distortion is not influenced by refraction and hence can be eliminated by standard in air distortion correction algorithms in advance. A set of parameters accounting for refraction is assumed to be known as well. These comprise the indexes of refraction of the involved media, which are expected to stay constant. Further known parameters are the perpendicular distance from the refractive interface to the center of projection, the camera's orientation towards this interface and the interface thickness.

Stepping back to the assumption of the underwater camera imaging a virtual object point, we show how

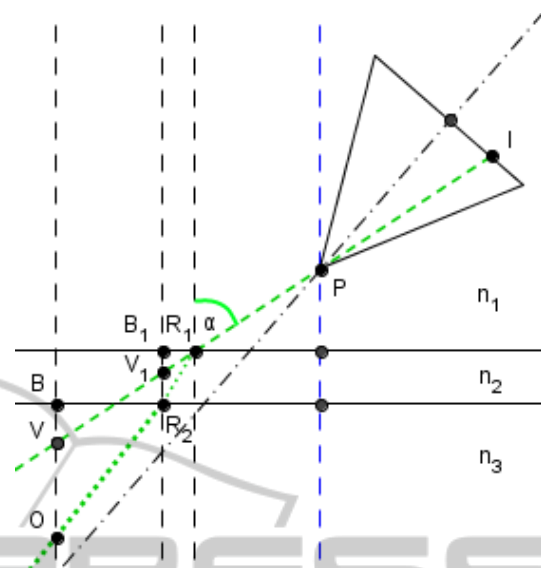


Figure 3: Geometric construction of the location of the virtual object point.

to infer virtual camera parameters following the pinhole camera model for the corresponding image ray using the virtual object point's location. These virtual parameters belong theoretically to a virtual camera imaging an underwater object point, as if the water was eliminated, to the same image point as the real underwater camera does. The image point in the virtual camera, its center of projection and the real underwater object point are collinear (see figure 4). As already mentioned before, refraction leads to the perception of an object being closer as it really is and hence being magnified. This corresponds directly to the location of the virtual object point. As a consequence, the virtual camera's focal length differs from the one of the real camera, because it has to compensate for this magnification. A well known limit case from physics is a ray with an incidence angle of 90 degrees. Only in this case the focal length can simply be multiplied by the refractive index of water to result in the corresponding virtual focal length (rule of thumb for underwater magnification). For incidence angles differing from this perpendicularity the computation gets more complicated. The virtual parameters don't just comprise focal length but also a new location of the center of projection and a new orientation to the refractive interface. The image's principal point is expected to stay constant and the skew factor is ignored.

The biggest problem is to find the location of the virtual object point V . More precisely, if one can find a rule to locate the virtual object point on the image ray relative to its real location on the refracted ray (see figure 3), one can infer the virtual camera parameters as will be shown. The result is a set of virtual parame-

ters per image ray. This can lead to a huge number of parameters, because the number of image rays corresponds to the number of image pixels. These parameters only depend on ray direction which stays constant from image to image, as long as the camera's position to the refractive interface stays fixed. They are independent of the imaged scene. Hence, it is possible to compute all parameters for a single image in a pre-computation step and reuse them for consecutive images. The number of parameters can be decreased if rays with the same properties are summarized. The only significant properties are the incidence angle to the refractive interface and the ray's angle to the optical axis of the camera.

3.2 Imaging Setup

For our experiments we generate an ideal imaging setup by using simulated underwater images rendered with Blender. Simulated images seem to be adequate for our effort to show the applicability of our theoretical approach for computation of virtual camera parameters. Advantages are the already known needed parameters and perfect perspective projection under the influence of refraction. The imaged scene and the general camera setup is not restricted. For convenience in evaluation we use a simple checker pattern on a plane with known dimensions and location as imaging target. The plane is located in a way that most of the image regions are covered by the pattern. This is especially useful to evaluate our algorithms in outer image regions, where distortions due to refraction get severe.

4 VIRTUAL CAMERA PARAMETERS

4.1 Location of Virtual Object Points

Refraction occurs on the way of the light from the emitting object point on the transition from water to glass and from glass to air according to Snell's law in a plane through the refractive interface's normal and the light ray. The way of the light depends on the distances it has to pass in the respective media, due to the fact that light always takes the path for which it needs the shortest time to travel (Fermat's law). Most of the times we do not know where the imaged object is located. But we do know the camera's center of projection and its orientation to the refractive interface. Hence, when looking along the path of light from camera direction, we can get an image ray from

pixel coordinates and also know its incidence angle to the refractive interface. Like can be seen in figure 3, the virtual object point V lies somewhere on the extended image ray. We start with the formula for refraction on a single interface:

$$\frac{n_1}{g} + \frac{n_2}{b} = \frac{n_2 - n_1}{r} \quad (1)$$

with g being the object distance, b being the image distance and r being the curvature radius of the interface. For a flat interface system we get $r = \infty$. After reorganization we end up with

$$b = -\frac{n_1}{n_2} * g. \quad (2)$$

This is what most physics textbooks teach for the case of an incidence angle of 90 degree. In this case, there is no refraction just a magnification. Other incidence angles are not considered explicitly in most cases. This formula is used as approximation for small deviations from 90 degree. It is obviously independent of the incidence angle and depends on distances and the speed of light in the involved media. We assume that these dependencies do not change if the incidence angle varies and just a change in direction of the image ray and the refracted ray is happening. When we consider both media transitions with its refractions ($n_1 = 0$) using formula (2), we get

$$\overline{R_1V} = \left| -\frac{\overline{R_1R_2}}{n_2} - \frac{\overline{R_2O}}{n_2} \right| \quad (3)$$

for the distance from the incidence point R_1 to the virtual object point V on the extended image ray. For a geometrical representation with an arbitrary but fixed real object point we have all we need to illustrate the location of the virtual object point. As can be seen in figure 3 it is located directly above the real object point on the perpendicular of the interface. If we vary the incidence angle or the object position this stays apparently the same. This statement coincides with parts of the work of (Bartlett, 1984). The location of the virtual object point is a controversial topic in physics. For our purposes we assume that the virtual object point is always located exactly above the real object point on the perpendicular of the flat refractive interface. That this assumption holds is shown in an experimental way in a later section. Based on this assumption, one can relate the distances from the interface (perpendicular) to the virtual point and to the real point incorporating all three involved media by

$$\overline{BV} = \overline{BO} * \frac{\cos \alpha}{\sqrt{n_3^2 - \sin^2 \alpha}} + \overline{B_1R_2} * \frac{\cos \alpha}{\sqrt{n_2^2 - \sin^2 \alpha}} \quad (4)$$

like in (Bartlett, 1984) by simple trigonometric rules. This relationship stays the same for arbitrary locations of the real object point on the same refracted

ray, which can be utilized for depth-independent calculations in the following sections.

After revisiting this concept to determine the location of the virtual object point, we show how to use it to infer the virtual camera parameters in the next subsection.

4.2 Parameter Computation

The computation of the virtual camera parameters is illustrated geometrically in figure 4. As refraction happens in a plane and following the results of (Agrawal et al., 2012), the virtual center of projection P' lies on the flat interface's normal through the real center of projection P (axial camera). The point is determined by the intersection of the rearward extended refracted ray (green dotted line turning into red) and that normal. As we know the angle β from the dot product of the image ray and the interface's normal in the camera's coordinate system as well as the distances $\overline{N_1N_2}$ corresponding to the interface thickness and $\overline{PN_1}$ corresponding to the perpendicular displacement of the center of projection from the interface, we can compute nearly all we need for parameter computation by simple trigonometric rules. Further refractive angles β' and β'' can be determined by Snell's law. Because of perpendicularity, the virtual center of projection P' turns to an easy computable distance. Now the location of the virtual object point V is incorporated. Since it is located directly above the real object point and their relationship is depth-independent we define it to be located exactly on the surface between water and glass. This fixation makes further simple trigonometric calculations possible.

As we know the angle α of the image ray to the optical axis of the camera from image coordinates and focal length, we know all the angles and distances illustrated in figure 4 except for the virtual focal length f' and the virtual camera's orientation. This orientation is conditioned by the angle α' in an ambiguous way. For determination of this focal length and orientation we need the rules for magnification of lenses from physical optics. In figure 4 both, the real (black triangle) and the virtual camera (red triangle) are illustrated. We want our real object O to appear at the exact same pixel position on the virtual camera's image sensor (I') as is the virtual object point V on the real camera's sensor (I). It has to be in the correct magnification which is realized by the virtual focal length and correct positioning of the virtual camera's optical axis. The virtual optical axis is determined by angle α' . From α' and r the virtual focal length f' can be easily calculated. For the calculation of α' we found out that the distances perpendicular to the re-

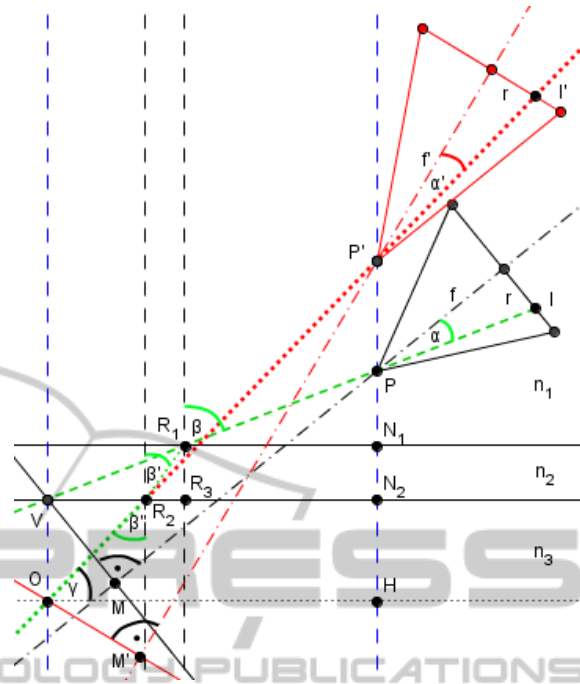


Figure 4: Geometric construction of the virtual parameters.

spective optical axis (MV and $M'O$) have to be equal, so that magnification works properly. Furthermore, by knowing angle α and the distances VP and OP' one can calculate α' by

$$\alpha' = \arcsin \frac{\sin \alpha * \overline{VP}}{\overline{OP'}}. \quad (5)$$

In contrast to refraction, which happens in a plane, the real and the virtual optical axis needs not to be located in that plane. The virtual optical axis has an ambiguous location, because it is just determined based on an angle α' to the respective ray. Hence, it can be located on a position anyway around the ray. This is not really a problem because of the fact that the pixel position of the ray in the respective image is not altered by this and the virtual parameters are calculated for this ray only. An arbitrary but matching virtual orientation can be computed with angle α' and the definition of the dot product as the angle between two vectors. One being the refracted ray and the other being the optical axis with two degrees of freedom. Based on the vector of the optical axis both missing coordinate axes can be computed in a similar way.

These virtual parameters essentially convert underwater imaging into imaging in air. If the camera is oriented perpendicular it leads to some simplifications during computation.

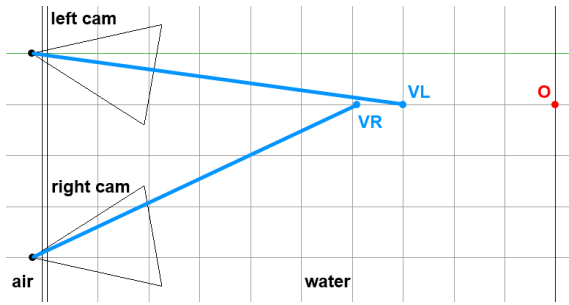


Figure 5: Stereo setup with different virtual object points.

5 3D-RECONSTRUCTION

In this experiment we use the concept for the relation between the location of virtual object points and real object points in a stereo 3D reconstruction problem. This should underline the applicability of this concept. Furthermore, the results are compared with the results of a stereo 3D reconstruction based on a naive in-situ stereo camera calibration ignoring refraction.

A stereo camera system is generated with Blender as can be seen in figure 5. The cameras are located 40 cm apart in a horizontal converging formation of 10 degree per camera. The perpendicular distance to the flat refractive interface with a thickness of 1cm amounts to 2cm for each camera. The refractive indexes are respectively 1 for air, 1.6 for glass and 1.33 for water. The focal length of both cameras is 27mm, with an image resolution of 1920x1080, square pixels and a horizontal sensor size of 22.3mm. Hence, all needed parameters are known in advance (corresponding to camera calibration in air) and radial image distortion can be set to zero. Both cameras image a plane with a checker pattern at a certain distance. The checker corners on that plane are used as feature points and their respective 3D locations are known. We tried to cover as much of the overlapping image region with the pattern. For each corresponding feature pair the respective image ray is calculated in a left-handed world coordinate frame with its origin on the foot of perpendicular of the left camera on the water-sided interface. The z-axis is pointing into the water, the y-axis points upward and the x-axis to the left. The two rays are emitted from a different virtual object point (VL and VR). However, both rays correspond to the same real object point O. The two virtual object points are not likely to intersect in the same z-value as long as their respective rays have different incident angles. What we are able to do is to compute the intersection of just the x- and y-values of both rays. The results are differing in their z-values as can be seen exemplary in figure 5. Now we use formula

(4) to compute the z-value of the real object point. The two new z-values should be nearly the same and we take their mean as object depth. The x- and y-values stay the same. With this easy method we have inferred the 3D coordinates of our object from just a virtual object point and refraction is handled physically plausible.

6 RESULTS

The results of our computation of virtual camera parameters are tested in an experimental way. The rendering sequence to check if our computed virtual camera parameters match the situation works as follows. We render an underwater image of our target with Blender with known parameters. We compute the virtual parameters for one feature point. Afterward, we use these parameters in Blender to render a new image of our target, but this times in air. The result should be an image with the feature point at exactly the same image location and in the same magnification as in the underwater image. This feature point is now the result of a perspective projection and refraction is eliminated for this particular image pixel. The camera is imaging a plane with a checker pattern in an underwater environment. The refractive indexes are respectively 1 for air, 1.6 for glass and 1.33 for water. The interface has a thickness of 1cm and the camera is placed 2cm in perpendicular direction away from it with a horizontal angle of 10 degree. Its focal length is 27mm. This matches the left camera in figure 5. Because of the required exact placement and configuration of the virtual camera, this can not be evaluated in the desired accuracy with real image setups in a reasonable way.

One rendered result can be seen in figure 6. The corresponding feature points are marked with a circle. Manual visual evaluation results in a difference of zero pixel between both feature points. The green lines are drawn supplementary to illustrate the distortions in the underwater image and the truly straight chessboard lines in the in air image. Because of the already mentioned ambiguous orientation of the virtual camera, the in air rendered image is rotated. The pixel position is not affected by this as can be seen and as was explained before. The virtual focal length for this case is 36.632mm, the virtual center of projection is at a distance of 2.608cm from the refractive interface and the camera's rotation matrix amounts to

$$R = \begin{pmatrix} 0.9718 & 0.2121 & 0.1027 \\ -0.0909 & -0.0644 & 0.9938 \\ 0.2174 & -0.9751 & 0.0433 \end{pmatrix}.$$

Further tests on several random feature points re-

Table 1: 3D reconstruction errors

	IN-SITU(1m)	IN-SITU(2m)	OUR(1m)	OUR(2m)
3D Error	6.831cm	13.559cm	0.32cm	1.074cm
x-Error	6.571cm	12.92cm	0.08cm	0.15cm
y-Error	0.076cm	0.152cm	0.035cm	0.077cm
z-Error	1.714cm	3.65cm	0.285cm	1.042cm

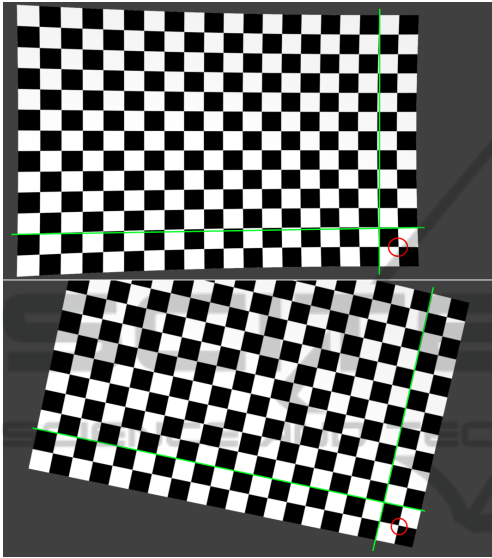


Figure 6: Comparison of the rendered underwater image (top) and the inferred in air rendering (bottom) with the corresponding ray (image pixel) marked by the red circle.

sulted in a mean deviation of at most 1 pixel. This shows that our method is well applicable for our scenario.

For stereo 3D reconstruction we used 204 feature points on a plane at a distance of 1m and 228 feature points on a plane at a distance of 2m from the refractive interface. The planes are parallel to the interface and all 3D locations of the feature points are known in advance. The results of our method and the results of a stereo 3D reconstruction based on a naive in-situ stereo camera calibration ignoring refraction are compared in table 1. The denoted errors are the 3D mean euclidean distance as well as the euclidean distances per coordinate direction between measured and real 3D points. Our results are significantly better than those of the in-situ method. The huge error in x-direction of the in-situ method amounts from false relative orientation parameters from in-situ stereo camera calibration. The ignored magnification by refraction leads to a shift of the camera behind its real position and to a smaller angle in the converging camera setup. This false camera configuration somehow compensates the triangulation error in z-direction at the cost of a shift in x-direction leading to an overall severe error in 3D location. On the contrary, our val-

ues match the 3D locations at this comparatively large imaging distances pretty well in all dimensions.

7 CONCLUSIONS

We presented a new method to convert an underwater image to imaging conditions in air with the aid of a set of virtual camera parameters for each image ray. Rays with the same properties can be summarized. Our method is based on rules of physical optics. The virtual parameters can be computed for one image in a pre-processing step. They can be reused for every consecutive image from that camera. With known virtual parameters, computer vision algorithms relying on the pinhole camera model can now be executed for the underwater images. In an experimental way, we show that our method matches our imaging conditions. Our results are tested on simulated image data allowing for ground truth comparison. This procedure shows that our theoretical results are correct and applicable. Our underwater imaging model makes it possible to infer parameters of an underwater camera from its calibration in air. Hence, we avoid a cumbersome and expensive in-situ calibration.

In a further experiment we show that our used concepts can be incorporated into stereo 3D reconstruction. The results are significantly better than the results of a naive in-situ stereo calibration with following triangulation. This experiment underlines the applicability of our method for underwater imaging. Further validation on real image data and a comparison with naive in-situ, as well as with more mature calibration approaches is needed and is part of our future work.

REFERENCES

- Agrawal, A., Ramalingam, S., Taguchi, Y., and Chari, V. (2012). A theory of multi-layer flat refractive geometry. In *2012 IEEE Conference on Computer Vision and Pattern Recognition (CVPR)*, pages 3346 – 3353.
- Bartlett, A. A. (1984). Note on a common virtual image. *American Journal of Physics*, 52(7):640 – 643.
- Beall, C., Lawrence, B. J., Ila, V., and Dellaert, F. (2010). 3D reconstruction of underwater structures.

- In *2010 IEEE/RSJ International Conference on Intelligent Robots and Systems (IROS)*, pages 4418 – 4423.
- Brandou, V., Allais, A. G., Perrier, M., Malis, E., Rives, P., Sarrazin, J., and Sarradin, P. M. (2007). 3D reconstruction of natural underwater scenes using the stereovision system IRIS. In *OCEANS 2007 - Europe*, pages 1–6.
- Chang, Y.-J. and Chen, T. (2011). Multi-view 3D reconstruction for scenes under the refractive plane with known vertical direction. In *ICCV'11*, pages 351 – 358.
- Chari, V. and Sturm, P. (2009). Multiple-view geometry of the refractive plane. In *Proceedings of the 20th British Machine Vision Conference, London, UK*.
- Eustice, R. M., Pizarro, O., and Singh, H. (2008). Visually augmented navigation for autonomous underwater vehicles. *IEEE Journal of Oceanic Engineering*, 33(2):103–122.
- Ferreira, R., Costeira, J. P., and Santos, J. A. (2005). Stereo reconstruction of a submerged scene. In *Proceedings of the Second Iberian conference on Pattern Recognition and Image Analysis - Volume Part I, IbPRIA'05*, pages 102–109.
- Gedge, J., Gong, M., and Yang, Y. (2011). Refractive epipolar geometry for underwater stereo matching. In *2011 Canadian Conference on Computer and Robot Vision (CRV)*, pages 146–152.
- Gracias, N. and Santos-Victor, J. (2000). Underwater video mosaics as visual navigation maps. *Computer Vision and Image Understanding*, 79:66–91.
- Ishibashi, S. (2011). The study of the underwater camera model. In *OCEANS, 2011 IEEE - Spain*, pages 1–6.
- Johnson-Roberson, M., Pizarro, O., Williams, S. B., and Mahon, I. (2010). Generation and visualization of large-scale three-dimensional reconstructions from underwater robotic surveys. *Journal of Field Robotics*, 27(1):21–51.
- Jordt-Sedlazeck, A. and Koch, R. (2012). Refractive calibration of underwater cameras. In *Proceedings of the 12th European conference on Computer Vision - Volume Part V, ECCV'12*, pages 846–859.
- Ke, X., Sutton, M. A., Lessner, S. M., and Yost, M. (2008). Robust stereo vision and calibration methodology for accurate three-dimensional digital image correlation measurements on submerged objects. *Journal of Strain Analysis for Engineering Design*, 43(8):689–704.
- Kunz, C. and Singh, H. (2008). Hemispherical refraction and camera calibration in underwater vision. In *OCEANS 2008*, pages 1–7.
- Kunz, C. and Singh, H. (2010). Stereo self-calibration for seafloor mapping using AUVs. In *Autonomous Underwater Vehicles (AUV), 2010 IEEE/OES*, pages 1–7.
- Kwon, Y.-H. and Casebolt, J. B. (2006). Effects of light refraction on the accuracy of camera calibration and reconstruction in underwater motion analysis. *Sports Biomechanics / International Society of Biomechanics in Sports*, 5(2):315–340.
- Lavest, J. M., Rives, G., and Lapreste, J. T. (2003). Dry camera calibration for underwater applications. *Mach. Vision Appl.*, 13(5-6):245 – 253.
- Li, R., Li, H., Zou, W., Smith, R. G., and Curran, T. A. (1997). Quantitative photogrammetric analysis of digital underwater video imagery. *IEEE Journal of Oceanic Engineering*, 22(2):364–375.
- Maas, H.-G. (1995). New developments in multimedia photogrammetry. *Symposium A Quarterly Journal In Modern Foreign Literatures*, 8(3):150 – 5.
- McKinnon, D., He, H., Upcroft, B., and Smith, R. N. (2011). Towards automated and in-situ, near-real time 3-d reconstruction of coral reef environments. In *OCEANS'11 MTS/IEEE Kona Conference*.
- Meline, A., Triboulet, J., and Jouvencel, B. (2010). A camcorder for 3D underwater reconstruction of archeological objects. In *OCEANS 2010*, pages 1–9.
- Pessel, N., Opderbecke, J., and Aldon, M. J. (2003). An experimental study of a robust self-calibration method for a single camera. In *Proceedings of the 3rd International Symposium on Image and Signal Processing and Analysis, 2003. ISPA 2003*, volume 1, pages 522–527.
- Pizarro, O., Eustice, R. M., and Singh, H. (2009). Large area 3-D reconstructions from underwater optical surveys. *IEEE Journal of Oceanic Engineering*, 34(2):150–169.
- Sedlazeck, A. and Koch, R. (2011). Calibration of housing parameters for underwater Stereo-Camera rigs. In *Proceedings of the British Machine Vision Conference*, pages 118.1 – 118.11.
- Sedlazeck, A. and Koch, R. (2012). Perspective and non-perspective camera models in underwater imaging - overview and error analysis. In *Outdoor and Large-Scale Real-World Scene Analysis*, volume 7474 of *Lecture Notes in Computer Science*. Springer Berlin Heidelberg.
- Sedlazeck, A., Koser, K., and Koch, R. (2009). 3D reconstruction based on underwater video from ROV kiel 6000 considering underwater imaging conditions. In *OCEANS 2009 - EUROPE*, pages 1–10.
- Shortis, M., Harvey, E., and Abdo, D. (2009). A review of underwater stereo-image measurement for marine biology and ecology applications. In *Oceanography and Marine Biology*, volume 20092725, pages 257–292. CRC Press.
- Shortis, M. R. and Harvey, E. S. (1998). Design and calibration of an underwater stereo-video system for the monitoring of marine fauna populations. *International Archives Photogrammetry and Remote Sensing*, 32(5):792–799.
- Silvatti, A. P., Salve Dias, F. A., Cerveri, P., and Barros, R. M. (2012). Comparison of different camera calibration approaches for underwater applications. *Journal of Biomechanics*, 45(6):1112–1116.
- Telem, G. and Filin, S. (2010). Photogrammetric modeling of underwater environments. *ISPRS Journal of Photogrammetry and Remote Sensing*, 65(5):433–444.
- Treibitz, T., Schechner, Y., Kunz, C., and Singh, H. (2012). Flat refractive geometry. *IEEE Transactions on Pattern Analysis and Machine Intelligence*, 34:51–65.
- Yamashita, A., Kato, S., and Kaneko, T. (2006). Robust sensing against bubble noises in aquatic environments with a stereo vision system. In *Proceedings 2006 IEEE International Conference on Robotics and Automation, 2006. ICRA 2006*, pages 928–933.